Dimensional Measurement and Defect Detection Using Spatial Filtering

Abstract: A new method is described that utilizes coherent bandpass spatial filtering and subsequent superposition to form filtered images in which small differences in size and geometry of the original object are readily detected. The theoretical basis is discussed and experiments described in which signal ratios of about 10:1 are obtained for a diameter change of 2.5 percent of a clear circular disc. The method is used to process in parallel a 57-mm evaporation mask containing 12 000 holes, each being 0.1 mm in diameter. The size of each hole is accurately gauged and small imperfections are indicated in the filtered image.

Introduction

In recent years the techniques of optical data processing have found wide application in pictorial information processing [1], optical computing [2], pattern recognition [3], seismic processing [4], and other areas [5].

In many applications, high-density arrays containing large numbers of identical two-dimensional patterns are used. It is often required that each array element be fabricated to high precision and that all be free of defects. For such applications accurate dimensional gauging and reliable defect detection become mandatory.

Conventional scanning and comparison techniques are serial in nature and must be sufficiently sensitive to detect signals of low contrast. These methods are consequently slow and require large amounts of signal processing.

The techniques of optical data processing have been successfully applied to the detection of defects in two-dimensional arrays [6-8]. These techniques process information in parallel and produce high-contrast signals, permitting rapid, high-speed inspection.

In this paper a new technique is described that combines both accurate dimensional gauging and defect detection in a single wide-field optical system. The high-speed method of optical data processing is described in detail for arrays containing upwards of 10 000 identical holes or other circular patterns. Its generalization to more complex two-dimensional geometries is also discussed.

For the specific application described, the system is capable of gauging hole sizes to within ± 2 percent over a $2\frac{1}{2}$ -inch (5.7-cm) field. No pattern alignment is required

and, in contrast to other defect detection techniques [7, 8], the pattern array need not be periodic.

This application is based on the theory of bandpass spatial filtering described in detail elsewhere for both one- [9, 10] and two-dimensional objects [11].

The sections following describe the technique, its theoretical basis and its application to large-field arrays. The mathematics of the underlying theory is covered in the Appendixes.

Spatial filtering

• Optical data processing

The techniques of optical data processing are based on the diffraction theory of image formation, formulated by Abbé nearly 100 years ago; modern authors have reformulated and expanded them in terms of communication theory concepts [12, 13]. In these terms, all image formation can be considered mathematically to occur in two steps. First, a spatial frequency analysis (Fourier transform) is performed on the object. This is followed by a frequency synthesis of the transform to form the image [14, 15].

The optical system is shown in Fig. 1(a). Under coherent illumination, the first lens produces a Fraunhofer diffraction pattern in its back focal plane that is mathematically identical to the spatial Fourier transform of the object. The object is thus frequency-analyzed by the first lens and each point in the back focal plane represents a unique point in the two-dimensional spatial frequency domain. A second lens L_2 , placed a focal length f_2 be-

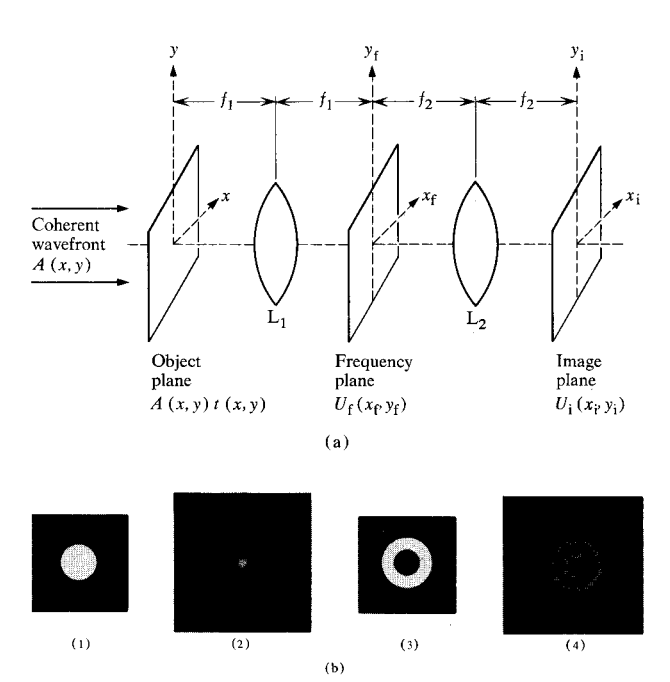


Figure 1 Basic optical system using spatial filtering for dimensional measurements and defect detection. (a) Configuration in which diffracted rays θ_1 and θ_2 are focused at a_1 and a_2 in the frequency plane. (b) Images of clear disc formed by bandpass spatial filtering: (1) object, (2) spectrum, (3) filter, and (4) filtered image.

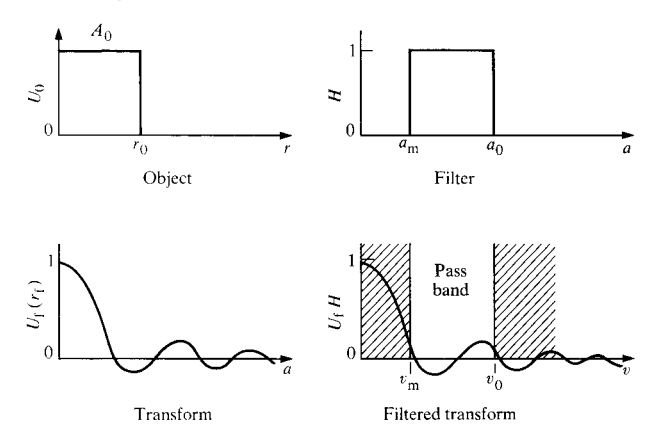


Figure 2 The bandpass filter and the relationship between the frequency spectrum and the physical sizes of the object and filter.

hind the transform plane, performs a second Fourier transform, which synthesizes the frequency spectrum into an image of the original object located a distance f_2 behind L_2 .

Spatial filtering is the process of modifying the signal from the object by selectively blocking points or regions in the frequency plane (back focal plane). By choosing the size, shape, orientation and location of the filter in the transform plane, selected information can be eliminated or suppressed, leaving only the desired information in the processed image. In this way, information is pro-

cessed in the spatial frequency domain, where it is in a convenient form to characterize and the desired data handling operation is easier to perform.

• Parallel processing

Another distinct advantage of the optical data processing method of Fig. 1(a) is the ability to process all signals in the input plane simultaneously and independently of location. This arises because

- 1. The same diffraction pattern amplitude is produced for an object independently of its location in the input plane.
- 2. The lens focuses all identical diffraction patterns into the same locations in the back focal plane.

In this way, elements in an array of like objects have the same frequency spectrum and hence produce the same spatial signal in the back focal plane.

Any modification of the focal plane signal simultaneously modifies the spectrum of every object element in the same way. The subsequent reimaging operation produces a filtered image of each object at a point corresponding to its original location in the object plane. This filtered image is produced by a single filter operating on all input objects in parallel.

• Bandpass spatial filtering of circular objects

The basic spatial filtering operations applied to a circular object (either clear on a dark field or dark on a clear field), as illustrated in Fig. 1(a), are

- 1. Collimated coherent monochromatic illumination of the object located in the front focal plane of lens L_1 (focal length f_1).
- 2. Fourier transform by L_1 .
- 3. Spatial filtering at back focal plane f_1 .
- 4. Fourier transform by $L_2(f_2)$.
- 5. Filtered image at f_2 from L_2 .

The effects of operations on a clear disc are illustrated in Fig. 1(b). A circularly symmetric bandpass filter is shown, which removes low-frequency components from the signal to produce the resulting filtered image.

A schematic representation of bandpass filtering and the relations to the object and its frequency spectrum are shown in Fig. 2. The amplitude spectrum of a clear disc of radius r_0 is $J_1(v)/v$, with $v=2\pi r_0 a/\lambda f_1$, where a is the radial distance in the focal plane, λ is the wavelength of the coherent radiation and J_1 is the first-order Bessel function. The quantities represented in Fig. 2 are defined and discussed in Appendix A. Two types of image dependence are found to exist: 1) For a fixed object, the image varies with the size and position of the passband, and 2) for a fixed filter, the image varies rapidly with the size of the object.

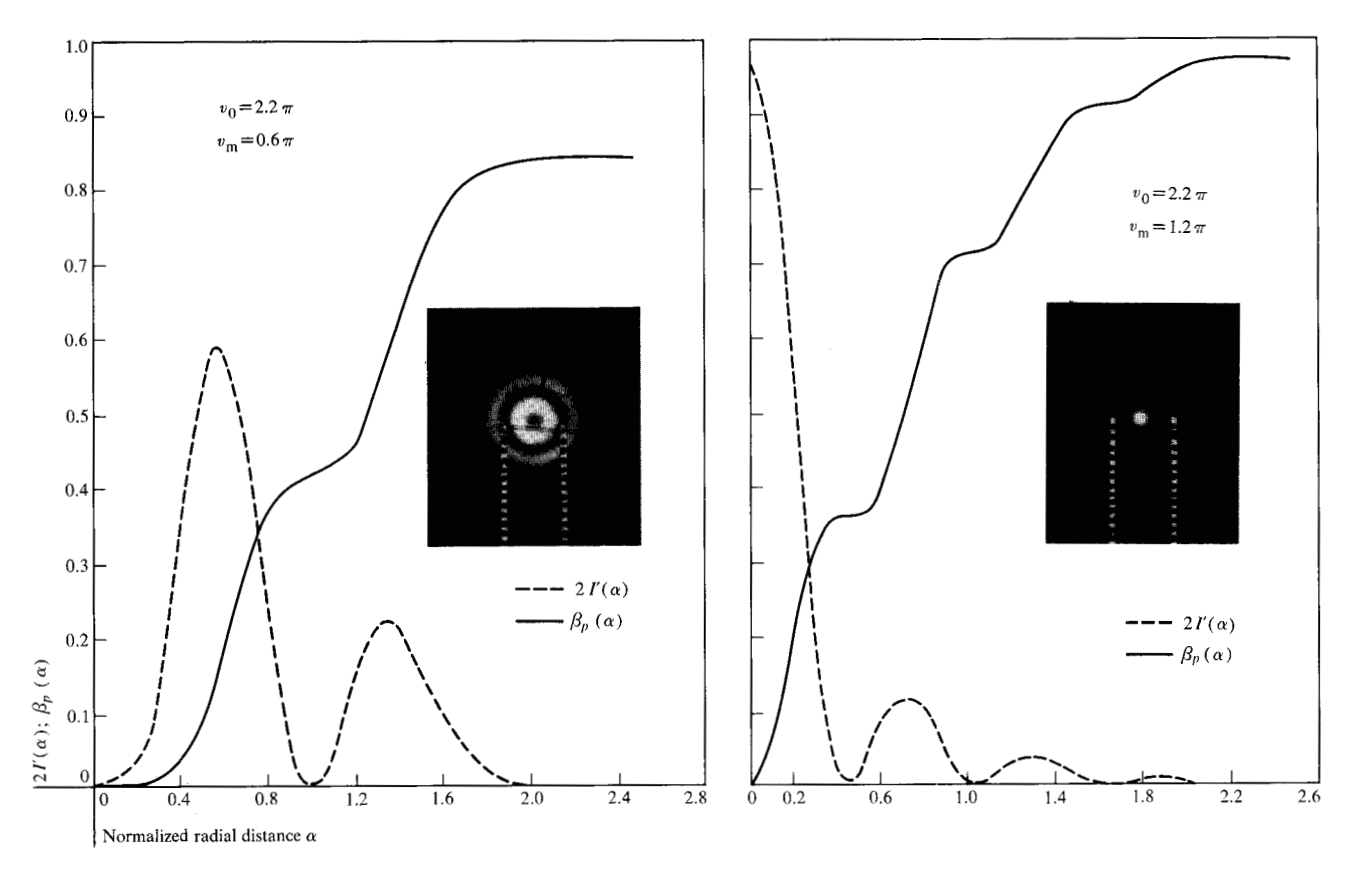


Figure 3 Filtered images for two different filters. Intensity I and enclosed energy β are shown as functions of position α . The dashed lines define the edge locations of the unfiltered images.

The filtered images for a fixed object (100- μ m disc) using two different filters are shown in Fig. 3. The filters chosen had the same high-frequency cutoff but differing low-frequency cutoffs. The high-frequency cutoff v_0 of each filter occurs at the position of the second zero of the spectrum $J_1(v)/v$ (at $v=2.2\pi$) and the low-frequency cutoffs $v_{\rm m}$ are located at one-half and one times the distance to the first zero (at $v=0.6\pi$, 1.2π). The images differ considerably in absolute intensity and in detailed energy distribution.

The filtered image intensity distribution $I'(\alpha)$ and enclosed energy $\beta_p(\alpha)$ calculated from the relations given in Appendix A are also shown in Fig. 3. Here α is the normalized image position r_i/r_0 . The image on the left in the figure has zero intensity at the center. In comparison with the image on the right, it has lower peak intensity and about half the enclosed energy within a region defined by the boundary of the original object at $\alpha=1$.

Applications

◆ Accurate dimensional detection

The filtered images described thus far pertain to the case of fixed object size and various filter passbands. An

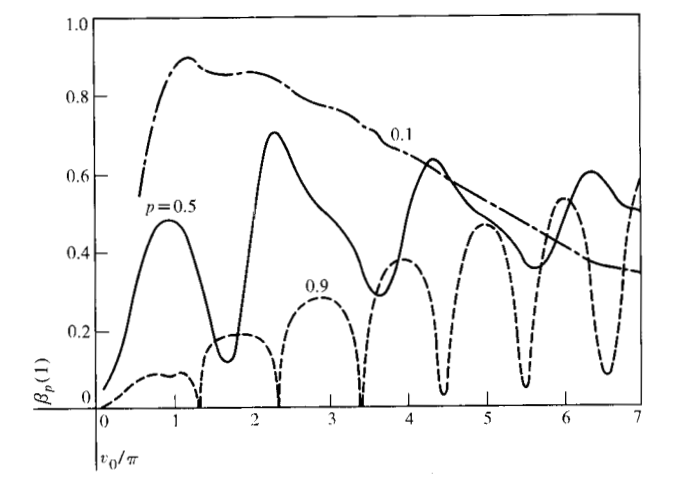


Figure 4 Enclosed energy within unfiltered image boundary $\alpha = 1$ for three different filters. Parameter p is the ratio of low-to high-frequency cutoff.

analogous sensitivity exists in a fixed filtering system when the object size is varied.

Figure 4 is a plot of the enclosed image energy β_p for various values of p, the ratio of low- to high-frequency cutoff. For a fixed system (i.e., fixed lens, wavelength

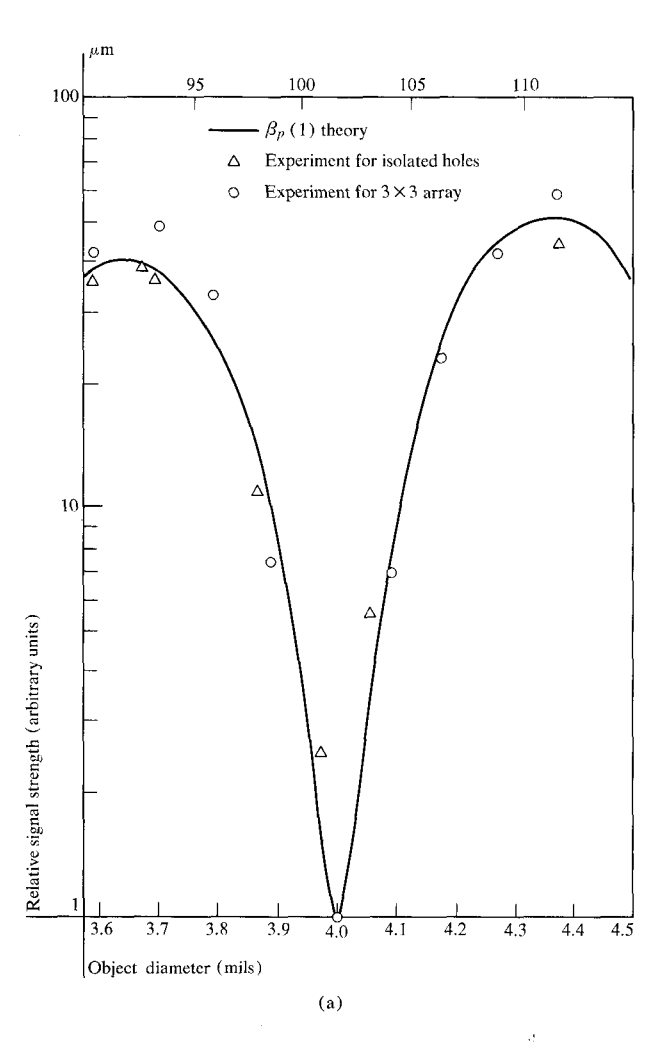
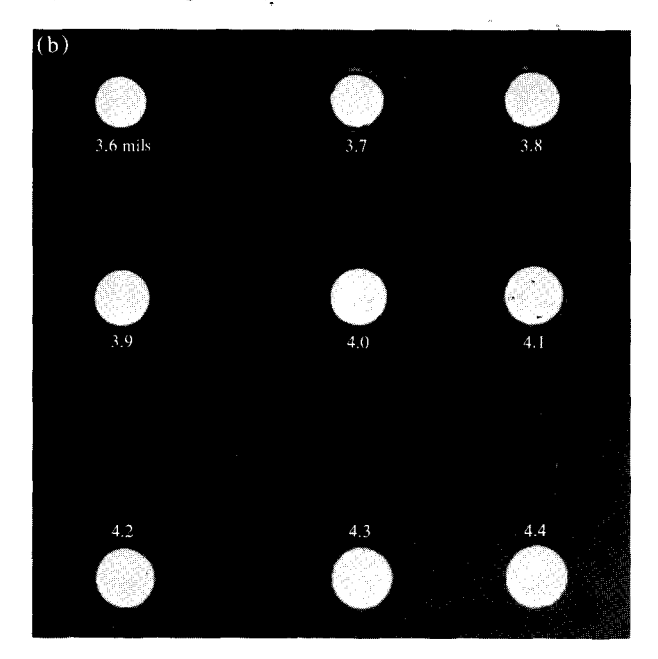


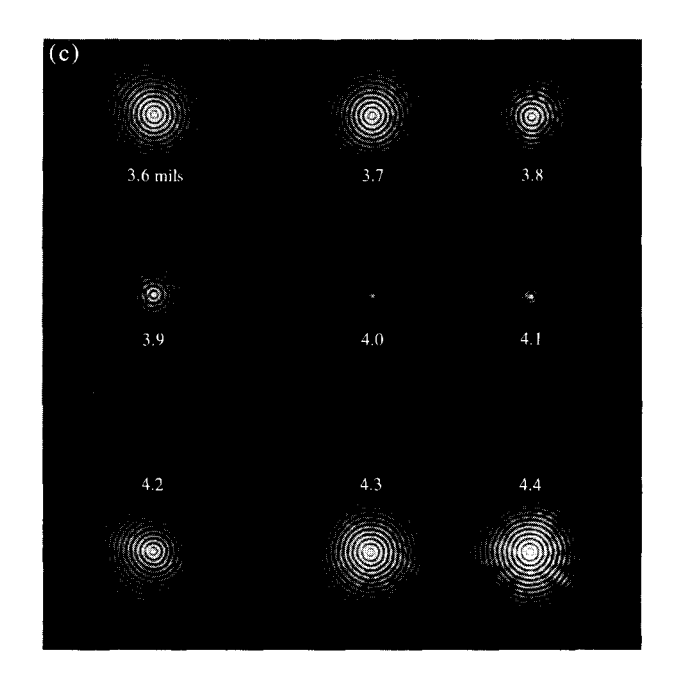
Figure 5 (a) Relative signal β_p (1) versus object size: Δ -Isolated objects. $o-3 \times 3$ Array [see (b)]. (b) 3×3 sample array. (c) Filtered image of (b).



and passband) this curve is a plot of image energy versus object size. In this plot for p=0.9, for example, there are a number of regions in the vicinity of the minima at which the scanned image energy is extremely sensitive to object size. It is thus possible, by appropriate choice of filter, to design a system that is selectively sensitive to an object of a given dimension by producing from it either a very weak or a very strong filtered image. This behavior of bandpass filtered images is utilized here for precise dimensional measurements.

The region about the minimum at $\alpha = 5.5$ for p = 0.9in Fig. 4 is expanded and shown in Fig. 5(a). Here the system parameters are chosen so that the minimum occurs for a disc 4 mils (0.1 mm) in diameter. As can be seen, a size change of \pm 0.1 mil (2.5 μ m) corresponds to a change in signal amplitude by a factor of nearly 10. The open dots in the figure plot the signals obtained from the 3×3 array shown in Fig. 5(b). The clear discs shown in Fig. 5(b) vary from 3.6 to 4.4 mils (0.09 to 0.11 mm) in 0.1 mil steps. Their separations vary from 2 to 4 diameters. With the maximum sensitivity of the filtered image centered at 4.0 mils, this system can be used as an extremely sensitive hole-size gauge, with a tenfold signal increase for a 0.1-mil change in diameter. Even greater signal increases occur for greater deviations from the chosen design center.

This example could represent a typical inspection or measurement situation in which the central row is within tolerance and the upper and lower rows are out of tolerance. The filtered image for this array is shown in Fig. 5(c), where the indications of out-of-tolerance holes in the upper and lower rows are greatly enhanced compared



512

to those within tolerance. This photograph shows the sensitivity achievable with this system as a visual "go-no-go" gauge.

For use as a precise measurement system, Fig. 6 gives the actual signals obtained by scanning the central row.

Large-field optical processing

The data and filtered images described thus far were obtained using a pair of well-corrected laser collimator lenses. These lenses operate with the required amplitude and phase fidelity over about a 0.1-inch (2.5-mm) field, centered on axis, where the paraxial approximation is valid. If implemented over larger fields, the technique can have wide application.

An example of such a potential application is the 2.25-inch (5.7-cm) diameter evaporation mask shown in Fig. 7. It contains more than 10 000 holes, each being 4 mils (0.1 mm) in diameter and having a required tolerance of the order of \pm 5 percent. To apply this measurement technique over fields of this size, lenses specifically designed for optical data processing requirements are necessary. For such lenses, the frequency response must be independent of object position, and precise phase information must be maintained over the whole field, so that all object points can be processed in parallel. Any phase distortion in either the illuminating system or the actual imaging system will couple the signals from separate objects in the field and degrade the ability of the system to process each object independently.

These requirements are satisfied most directly by a symmetric, telecentric lens system of long focal length, an example of which is described in the work of Blanford [16]. Such a lens system was designed and fabricated by Tropel, Inc. and applied to the mask shown in Fig. 7.

An example of the performance of this lens system is shown in Fig. 8(a) for a system designed for a 4.3 mil (0.11 mm) nominal diameter. The measured signal is plotted as a function of dimension for objects located at the farthest off-axis position, 1.125 inches (2.8 cm) from center, and compared with the calculated sensitivity. The excellent agreement between theory and the observed data is a good indication of the detailed performance of the lens system.

• Expanded-range filter

From the response curves in Figs. 4, 5(a), and 8(a), it is clear that the signal minima repeat themselves for large departures from the chosen design minimum, thus limiting the range of unambiguous size gauging. By appropriate choice of filter passband, however, a design is possible, characterized by Fig. 8(b), which has a single minimum over a range approaching ± 100 percent of the design center. Here a two percent change in size pro-

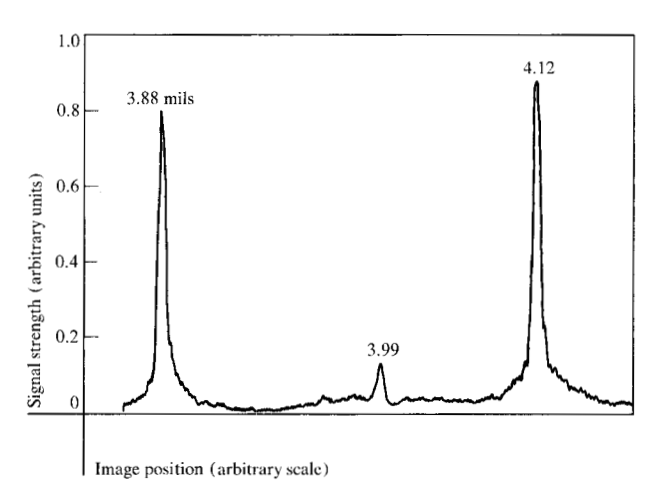
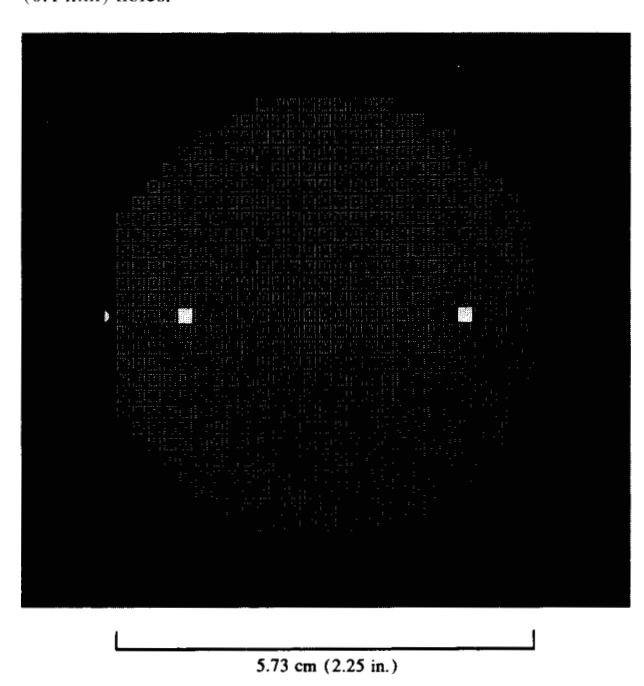
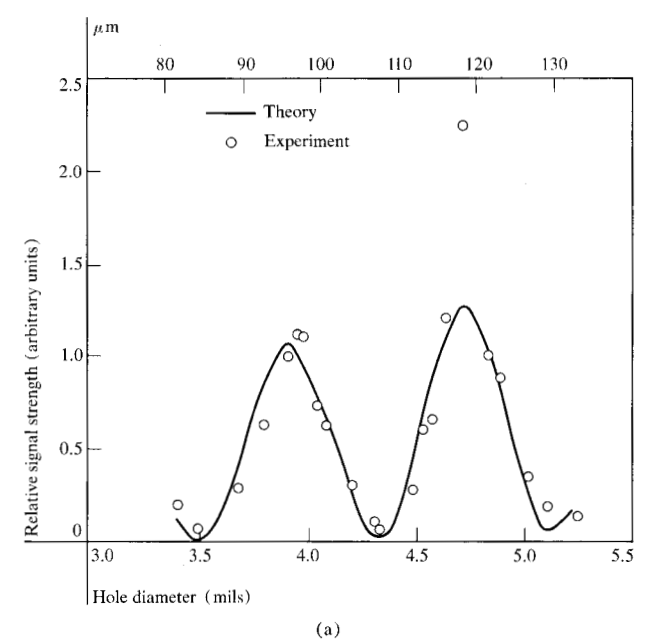


Figure 6 Scan across the central row of Fig. 5(c). The object-plane diameter of each hole is indicated.

duces a factor of 10 increase in signal with no possible ambiguity, over a range greater than 85 percent of the nominal size. For the 4-mil (0.1-mm) holes on the evaporation mask described previously, this design would apply uniquely over a range from 0.75 to 8 mils (0.019 to 0.2 mm). The choice of filter passband to give this improved selectivity and signal response is based on the mathematical analysis presented in Appendix B. The filter is chosen to pass those frequency components in

Figure 7 Evaporation mask containing 12 000 nominally 4-mil (0.1 mm) holes.





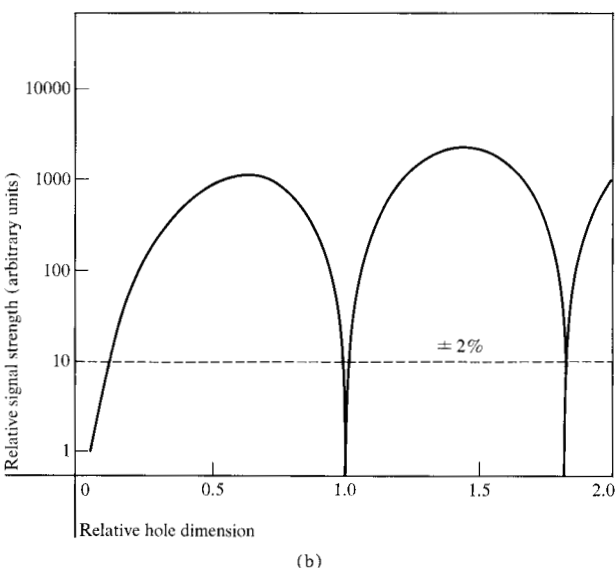


Figure 8 Example of system performance. (a) System response at extreme off-axis position. Design center is 4.3 mils (0.11 mm). (b) Response curve for expanded-range filter design.

which phases combine to produce total destructive interference at the center of the filtered image. Thus, even though the total energy passed by the filter is conserved and hence contained in the filtered image, this energy is spread or delocalized in the image plane to produce an image of extremely low energy density.

• Full-field filtered imaging

Using the expanded range filter characterized by Fig. 8(b) and the appropriate detector threshold, a full-field filtered image of the evaporation mask (Fig. 7) was obtained as shown in Fig. 9. Bright spots occur at each

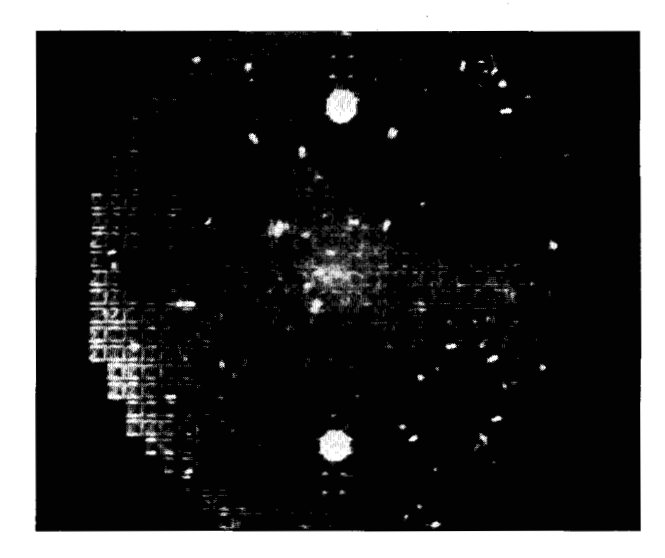


Figure 9 Full-field filtered image of evaporation mask.

hole location for each hole out of size by more than \pm 5 percent. It should be emphasized that for the circularly symmetric system described here, this full-field filtered image is obtained independently of position or orientation in the object plane so that the information processing is performed in a system truly free of alignment requirements.

In the full-field optical processing system developed here an argon laser beam is low-pass filtered to remove spatial noise and expanded to fully illuminate the object plane. The expanded beam must be carefully collimated to a fraction of a wavelength in order to produce an accurate frequency spectrum in the common focal plane of the two optical processing lenses. The spatial filter is then accurately centered in the frequency plane and the desired filtered image is produced in the image plane where it may be photographed or conveniently displayed on a CRT monitor. In the display mode, it is possible for an observer to obtain accurate size gauging simultaneously of all 12 000 holes in the mask in a system that is independent of any alignment tolerances beyond placement in the front focal plane.

• Defect detection

This concept can also be applied to defect detection. The sensitive gauging technique described thus far is based on our ability to control the superposition process forming the filtered image in such a way that images of patterns having a predetermined size and shape are formed by destructive interference of diffracted light waves. For all other geometries, the destructive interference is incomplete, and considerably more intense filtered images are formed.

Defective hole geometries, caused by either foreign materials or shape distortion, result in incomplete destructive interference, producing enchanced filtered images. As an example, we note the anomalously strong signal at 4.7 mils (0.12 mm) in Fig. 8(a) due to a partially blocked hole.

Many of the bright spots in the full-field filtered image are due to defects of this type. The closely separated bright spots shown on the left in Fig. 9 are due to the two defective geometries shown in Fig. 10(a). Both an undersized hole and a blocked hole are detected simultaneously by the system. In this case, the detected hole is about 20 percent undersized.

Figure 10(b) is an example of the amount of hole blockage detectable. Less than five percent of the total area transmits light, yet the system gives sufficient suppression of the ideal pattern to allow the signal from a defect of this type to be readily enhanced and easily detected. The image for such an object has higher intensity than that for an unobstructed hole in spite of the fact that it transmits considerably less energy.

The example in Fig. 10(c) shows a translucent defect covering the entire hole. Defects of this type give the strongest filtered image, since they cause only phase shifts that reduce the destructive intereference process, while having little effect on the total energy.

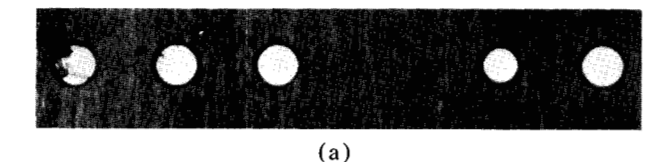
Summary

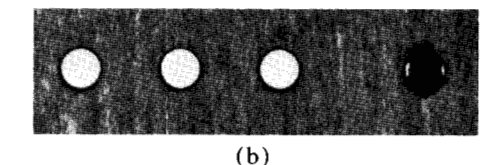
The theory of bandpass spatial filtering for circular objects and the effects of filter, object and system parameters on the resultant filtered image have been analyzed. The filtered image intensity was found to be extremely sensitive to all system parameters and in particular, for a fixed system, to object size and shape. From the basic analysis, a sensitivity curve was developed and verified experimentally.

It has been shown how filters may be designed to take advantage of this sensitivity to produce a system capable of accurate hole size gauging and defect detection. Though the application of spatial filtering to defect detection is not new, the approach to filter design presented here is a marked departure from existing methods.

In the present approach, the filter is chosen to create an extremely weak filtered image of the ideal (nondefective) pattern. This is done not by absorption of energy in the frequency plane, as is common to previous approaches, but rather by transmitting a precisely chosen portion of the frequency spectrum. Upon superposition in the filtered image this portion produces destructive interference and thereby an extremely weak filtered image.

The particular application of the method shown here is capable of size gauging and defect detection for each





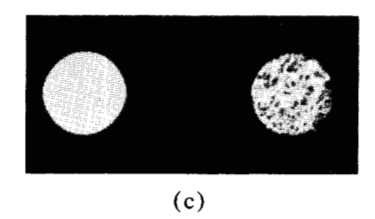


Figure 10 Typical defects detectable. (a) Blocked and undersize holes; (b) extreme blockage detectable; and (c) phase blockage detectable.

of 12 000 nominally 4-mil holes over a field of 2.25-inch diameter. The system was designed to fully exploit the large-field parallel processing potential of optical spatial filtering techniques, which permit high-speed, alignment-free processing of large amounts of information in a test object without moving parts.

The method does not require a periodic pattern array and can process any number of randomly distributed elements. These elements, however, must be nominally identical and separated by at least two diameters to eliminate interference between elements which may alter the precisely controlled superposition forming the filtered image. Furthermore, the optical processing is independent of orientation for circular objects only. Other shapes would use noncircularly symmetric filters and would require precise orientation of the object but would still possess no translational restriction. In this sense, the method is restricted in its ability to process large arrays in parallel to those containing like elements commonly oriented but distributed randomly.

By generalizing the filter design method presented here and by making use of all known information about the geometry of the patterns under study, it is possible to extend the method to more complex pattern recognition problems.

Appendix A: Bandpass spatial filtering of the circular disc

A generalized spatial filtering system is shown in Fig. 1(a). We consider an object with a two-dimensional amplitude transmission t(x, y) located in the front focal plane of lens L_1 of focal length f_1 , which is coherently illuminated by a collimated beam of wavelength λ and amplitude A(x, y) in this plane. The amplitude distribution in the back focal plane of L_1 , denoted here by $U_f(x_f, y_f)$, is given by the Fourier transform of the transmitted amplitude, $t(x, y) \cdot A(x, y)$ [15].

The effect of filtering on the resultant image is obtained by multiplying the frequency spectrum $U_{\rm f}$ by the filter function H and taking a second Fourier transform to give a filtered image with amplitude $U_{\rm i}$.

• Image intensity distribution and enclosed energy.

For circular objects, we let r, r_1 , r_1 represent the radial coordinate in the object, focal and image planes, respectively. For a bright disk in the object plane of radius r_0 , illuminated by a field of uniform amplitude A_0 , the focal plane amplitude distribution is given by the well-known Airy diffraction pattern. This can be written in terms of the reduced coordinate v as $\lceil 17 \rceil$

$$U_{\rm f}(v) = A_0(\pi r_0^2) [2J_1(v)/v], \tag{A1}$$

where
$$v = 2\pi r_0 r_f / \lambda f$$
 (A2)

and J_1 is the first-order Bessel function.

In the current example, we consider bandpass filtering in which case the filter is defined in terms of v as

$$H = 1 \text{ for } v_{\text{m}} \le v \le v_{\text{o}},$$

$$H = 0 \text{ otherwise.}$$
(A3)

where $v_{\rm m}$ is the low-frequency cutoff and $v_{\rm 0}$ the high-frequency cutoff.

For circularly symmetric objects, the one-dimensional Hankel transform can be used [18], so that the filtered image amplitude distribution can be written as

$$U_{\rm i}(r_{\rm i}) = \frac{-2\pi}{j\lambda f_2} \int_{v_{\rm m}}^{v_0} U_{\rm f}(r_{\rm f}) J_0(2\pi r_{\rm i} r_{\rm f}/\lambda f_2) r_{\rm f} dr_{\rm f}. \tag{A4}$$

With the system magnification M given by f_2/f_1 and defining $\alpha = r_1/Mr_0$ to be the normalized image radial position, we obtain the normalized image intensity distribution $I'(\alpha)$ given by

$$I'(\alpha) = \frac{I_{1}(\alpha)}{(I_{0}/M^{2})} \left| \int_{v_{0}}^{v_{0}} J_{1}(v) J_{0}(\alpha v) dv \right|^{2}, \tag{A5}$$

where

$$I_0 = A_0^2$$
 and

$$I_{i}(\alpha) = |U_{i}(\alpha)|^{2}$$
.

Bandpass filtered images can further be characterized by determining the amount of energy enclosed within a given circular sampling region of radius α . This quantity, which we denote by β , is used to determine the extent to which the image is spread beyond its ideal boundary at $\alpha = 1$ and thereby establishes the effectiveness of a filter in concentrating or spreading the image of a given object.

By incorporating the various specific system parameters in terms of the dimensionless variables α , v and M, the essential physical behavior of bandpass spatial filtering of a circular disc is given in terms of the integral in Eq. (A5). By evaluating this integral for various values of filter cutoffs it is possible to determine the effect of filter choice on the final filtered image in very general terms. Application to specific systems can then be made by directly interpreting the normalized variables in terms of the actual system parameters they represent.

The energy distribution within the filtered image depends on the input energy E_0 , on the fraction of this energy transmitted by the filter, and on the integrated intensity distribution. We thus define the parameter $\beta_p(\alpha)$ to be that fraction of the total energy transmitted by the filter and contained within a radius α in the image.

The quantity $\beta_p(\alpha)$ then becomes

$$\begin{split} \beta_{p}(\alpha) &= \frac{2E_{0} \int_{0}^{\alpha} I'(\alpha) \alpha d\alpha}{2E_{0} \int_{v_{\text{m}}}^{v_{0}} \left[J_{1}(v)/v\right]^{2} v dv} \\ &= \frac{\int_{0}^{\alpha} I'(\alpha) \alpha d\alpha}{\frac{1}{2} \left[J_{0}^{2}(v_{\text{m}}) + J_{1}^{2}(v_{\text{m}}) - J_{0}^{2}(v_{0}) - J_{1}^{2}(v_{0})\right]}, \end{split} \tag{A6}$$

where the denominator is the energy transmitted by the filter and is obtained by squaring and integrating Eq. (A1) over the filter passband.

To determine the effects of different filters, $I'(\alpha)$ and $\beta_p(\alpha)$ have been calculated for various combinations of high- and low-frequency cutoffs. Figures 11(a) and 11(b) show the results of this calculation of $I'(\alpha)$ and $\beta_p(\alpha)$ for $v_0=2.2\pi$ and four values of $v_{\rm m}$ within the primary diffraction lobe. From these figures, as well as from similar results obtained with other values of $v_{\rm m}$ and v_0 , it is clear that choice of filter cutoffs can dramatically affect the filtered image. By properly choosing the cutoffs, the image intensity can be peaked while image spread is minimized.

• Fixed filter with variable object size

Figures 11(a) and 11(b) represent the effects of various filters on a fixed object. In characterizing the effects of bandpass filtering it is useful to determine the degree of image sharpness as object size is varied for a fixed filtering system. This can be done by evaluating the enclosed

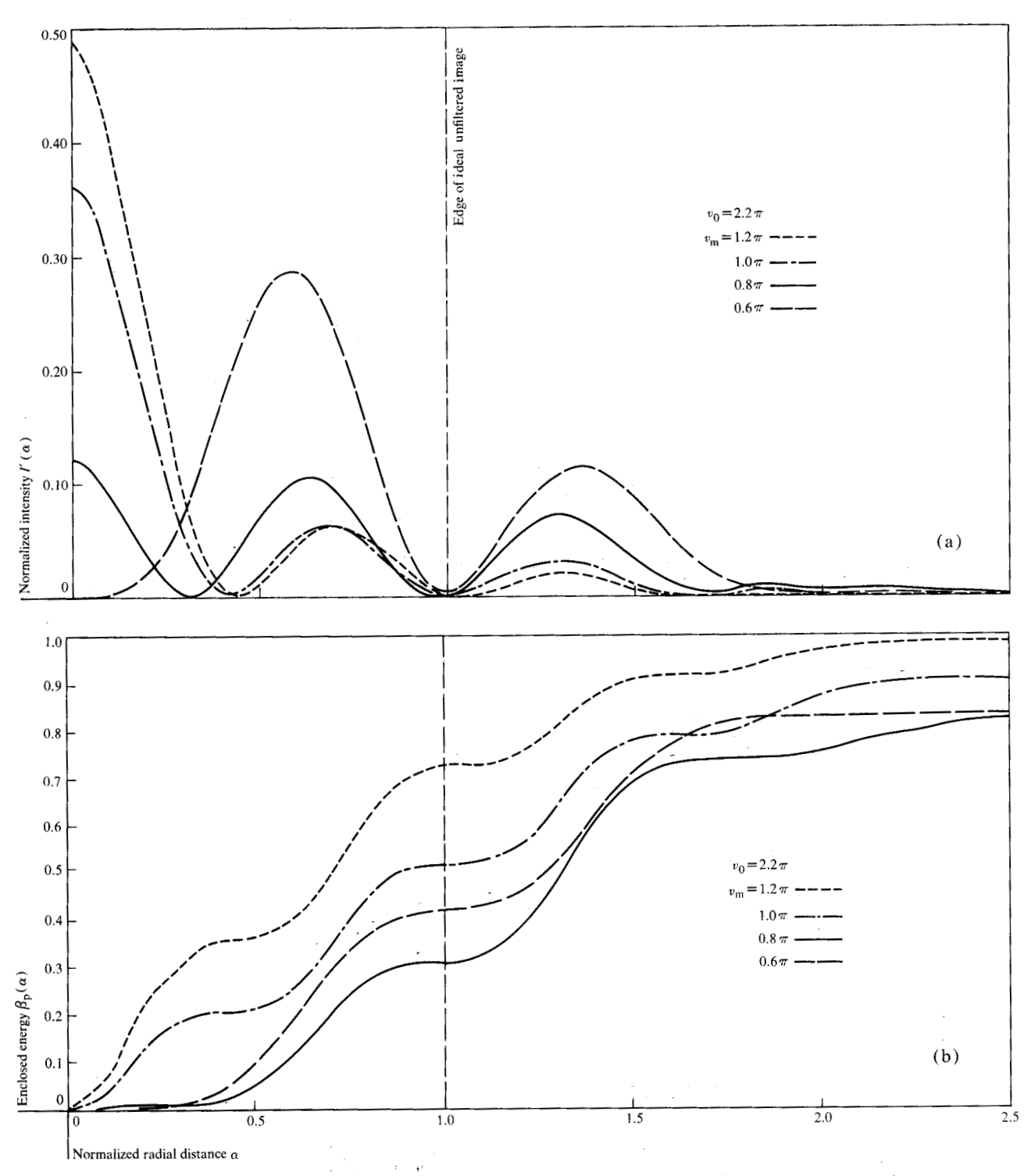


Figure 11 Calculated curves of (a) normalized image intensity and $I'(\alpha)$ and (b) enclosed image energy $\beta_p(\alpha)$ for a fixed high-frequency cutoff, $v_0 = 2.2\pi$, and several values of low-frequency cutoff. v_m .

image energy in a fixed sampling region defined, for example, by the boundary of the unfiltered image at $\alpha=1$. This parameter $\beta_{p}(1)$ is plotted in Fig. 4 as a function of v_{0}/π (proportional to r_{0}) for various values of $p=v_{m}/v_{0}$.

The value p = 0.9, for example, clearly portrays the degree to which energy concentration in the filtered image of a fixed spatial filtering system is strongly dependent on object size.

Appendix B: Method of filter design

To produce the delocalization of the filtered image that resulted in the high sensitivity to object size, the filter is chosen to produce zero intensity at the center of the filtered image.

At the image center $\alpha = 0$ and

$$I'(0) \propto \bigg| \int_{v_{\rm m}}^{v_0} \! J_1(v) \, J_0(0) dv \bigg|^2.$$

Noting that $J_0(0) = 1$ and that

$$\int_{v_{\rm m}}^{v_0} J_{_{I}}(v) \, dv = J_{_{0}}(v_{_{0}}) \, - J_{_{0}}(v_{\rm m}), \tag{B1} \label{eq:B1}$$

we have I'(0) = 0 when

$$J_{0}(v_{0}) = J_{0}(pv_{0}). \tag{B2}$$

This is the condition which must be satisfied for the object size whose image it is desired to suppress. Both graphic and numerical techniques can be applied to determine the appropriate values of p and v_0 which satisfy (B2). The wide range sensitivity curve of Fig. 8(b) was obtained with the values p=0.9165 and $v_0=4.0$.

Analogous filter design conditions are possible for other well-defined two-dimensional geometries. For the case of rectangles, for example, the Bessel functions used here are replaced by functions of the type $\sin v/v$ and $\cos v/v$ and their integrals from which design conditions analogous to Eq. (B2) can be derived.

Acknowledgments

We acknowledge the work of Gertrude Kappel, Robert Hill, Leonard Karstadt, and Frederick Koverda, who assisted throughout various phases of the development.

References

- 1. Optical and Electro-Optical Information Processing, J. T. Tippett, ed., The MIT Press, Cambridge, Mass., 1965.
- 2. A. Vander Lugt, in Ref. 1, Ch. 7.
- 3. G. Stroke, IEEE Spectrum 9, 24 (December 1972).
- 4. M. B. Dobrin, IEEE Spectrum 5, 59 (September 1968).
- 5. A. Vander Lugt, Optica Acta 15, 1 (1968).
- 6. E. S. Mathisen, *IBM Technical Disclosure Bulletin* 10, No. 7, 970 (December 1967).
- 7. L. S. Watkins, Proc. IEEE 57, 1634 (1969).
- 8. P. Will and K. Pennington, Appl. Optics 10, 2097 (1971).
- 9. K. G. Birch, Optica Acta 15, 113 (1968).
- 10. K. G. Birch, Optica Acta 17, 43 (1970).
- 11. A. Flamholz and G. Kappel, J. Opt. Soc. Am. 61, 1548(A) (1971).
- 12. L. O'Neill, IRE Trans. Information Theory IT-2, 56 (1956).
- L. J. Cutrona et al., IRE Trans. Information Theory, IT-6, 386 (1966).
- 14. J. E. Rhodes, Jr., Am. J. Phys. 21, 337 (1953).
- 15. J. W. Goodman, Introduction to Fourier Optics, McGraw-Hill Book Co., Inc., New York, 1968.
- B. Blanford, in Optical Instruments and Techniques, J. H. Dickson, ed.; Oriel Press, Newcastle, England, 1970, p. 435
- 17. M. Born and E. Wolf, *Principles of Optics*, 2nd ed., The Macmillan Company, New York, 1964.
- 18. R. Bracewell, *The Fourier Transform and its Application*, McGraw-Hill Book Co., Inc., New York, 1968.

Received April 13, 1973

The authors are located at the IBM System Products Division Laboratory, East Fishkill (Hopewell Junction), New York 12533.